EXPERIMENTAL IDENTIFICATION OF CONFIGURATION DEPENDENT LINKAGE VIBRATION IN A PARALLEL ROBOT USING SMART MATERIAL ACTUATORS AND SENSORS

Xiaoyun Wang and James K. Mills
Department of Mechanical and Industrial Engineering
University of Toronto, 5 King's College Road, Toronto, Ontario, Canada, M5S 3G8
Contacts: xiaoyun.wang@space.gc.ca, mills@mie.utoronto.ca

Received August 2006, Accepted March 2007
No. 06-CSME-35, E.I.C. Accession 2954

ABSTRACT

A new lightweight planar parallel robot is designed to achieve high acceleration and execute high-speed pick and place tasks. However, due to the lightweight structure of the system, unwanted structural vibrations are induced during motion of the platform. This work focuses on the investigation of the characteristics of this structural vibration utilizing distributed Lead Zirconate Titanate (PZT) transducers. Experimental Modal Analysis (EMA) tests were performed on an experimental three degree of freedom planar parallel robot with one flexible linkage, for cases in which the robot is stationary and in motion. For both cases, configuration dependency of link structural vibration is investigated by performing EMA in different configurations using different combinations of transducers. It is observed that FRFs obtained for the case in which the robot is in motion have more complex frequency compositions and more significant configuration-dependency than those in which the robot is stationary. However, the two groups of analyses exhibit two nearly identical most-significant modes. Based on this observation, the transfer function from motor inputs to linkage vibration is simplified permitting an linear active vibration controller to be used.

IDENTIFICATION EXPERIMENTALE DES VIBRATIONS D'UN MECANISME SELON LA CONFIGURATION DANS UN ROBOT PARALLELE EN UTILISANT DES ACTUATEURS ET DES SENSEURS INTELLIGENTS

RESUME

Un nouveau robot parallèle planaire léger est conçu pour obtenir des accélérations élevées et exécuter des tâches de transfert à grande vitesse. Cependant, en raison de la structure légère du système, des vibrations structurales non désirées sont induites pendant le mouvement de la plate-forme. Ce travail se concentre sur la recherche des caractéristiques de cette vibration structurale en utilisant des capteurs distribués de titanate de zirconium de plomb (PZT). Des essais modaux expérimentaux ont été réalisés sur un robot parallèle planaire expérimental à trois degrés de liberté avec un mécanisme flexible, pour les cas dans lesquels le robot est stationnaire et en mouvement. Pour ces deux cas, l'effet de la configuration sur la vibration structurale du mécanisme est étudié par des essais modaux expérimentaux dans différentes configurations en utilisant différentes combinaisons des capteurs. On observe que les réponses fréquentielles obtenues pour le cas dans lequel le robot est en mouvement ont des spectres fréquentiels plus complexes et l'influence de la configuration est plus significative que dans les cas où le robot est stationnaire. Cependant, les deux groupes d'analyses identifient les deux modes les plus significatifs de façon presque identique. Basée sur cette observation, la fonction de transfert des entrées du moteur aux vibrations du mécanisme est simplifiée pour permettre à des contrôleurs actifs linéaires d'être utilisés.

1. INTRODUCTION

Parallel robots have been used in a myriad of different applications, providing rapid multi-axis motion [1]. In recent years, parallel robots have gained interest for applications in various manufacturing industries, i.e. precision optics, nano-manipulation, and surgery, due to a number of desirable advantages over serial robots: (1) better dynamic behavior; (2) smaller size; (3) reduced accumulated error; and (4) better repeatability and reliability. A "smart parallel robot", shown in Figure 1, featuring the integration of parallel mechanism architecture, distributed sensing and active vibration control of linkage vibration using PZT components, is proposed [2]. This robot has been designed for electronic manufactory tasks, including wire-bonding and electronic-component pick-and-place tasks. These tasks require high-speed motion, in particular fast acceleration and deceleration, to increase the through-put in manufacturing tasks. The *P-R-R* (*Prismatic-Revolute-Revolute*) kinematic architecture of the robot was selected based on an optimal workspace criterion [3]. In order to identify and control structural vibration of the robot linkages, accompanying rapid acceleration and deceleration of the robot, PZT transducers are bonded to the surfaces of flexible linkages.

Recent emergence and development of smart materials provides a new potential solution for vibration suppression [4]. "Smart structures" utilize micro-controllers and distributed or embedded smart material based actuators and sensors to dynamically alter the behavior of structural dynamics which actively suppresses vibration in high-speed machines. Different from traditional passive control techniques [5]-[8], the smart structure control approach permits control of unwanted structural vibration where flexible deformation is dynamically coupled with nonlinear rigid-body motion, exhibiting both configuration-dependent and nonlinear behavior. This paper presents a foundation for experimental identification and control of unwanted structural vibrations, using smart material transducers applied to a smart planar parallel robot.

In the literature, researchers [9]-[13] have introduced PZT material for active vibration control of flexible mechanisms. Based on an analytical modal model, Sung *et al.* [9]-[10] numerically and experimentally investigated the use of a single PZT sensor and PZT actuator, i.e. a single-input single-output (SISO), to suppress linkage vibration of a four-bar linkage mechanism. Choi *et al.* [11] simulated linkage vibration control of a flexible mechanism using piezoelectric films using dynamic models developed with the Assumed Mode Method (AMM). Substantial research has been undertaken in dynamic modeling of structural vibrations in parallel robots. It is noteworthy that the choice of modal sets of flexible linkages remains an open research problem. Kang and Mills used a pinned-free modal set to model structural vibration of a linkage in a parallel robot [14]. de Jalón and Bayo [15] suggested pinned-pinned boundary conditions for flexible mechanisms with closed loops. In [2], the authors employed a substructure dynamic modelling approach, which is based on a Craig-Bampton modal set. Validation of numerical dynamic models and development of active linkage vibration control of flexible mechanisms mandate experimental identification of structural vibrations of parallel robot using distributed transducers.

Design of an effective vibration controller mandates that the structural vibrations in flexible linkages must be precisely modeled. A feature of modeling flexible-link parallel robots is that it is cumbersome to develop a dynamic model using independent coordinates because of the closed-loop kinematic structure. In order to investigate the control of linkage vibration more clearly and thoroughly, vibration characteristics of the parallel robot must be studied experimentally. The main focus of this paper is to experimentally identify configuration-dependent vibration characteristics of a flexible linkage, instrumented with PZT transducers, in various configurations and conditions so that active vibration controllers may be designed.

The paper is organized as follows. The EMA procedure used in this work is described in Section 2 along with a brief review of experimental studies of flexible mechanisms. In Section 3, FRF formulations using PZT transducers and formulation using rigid-body motion are developed. The source of configuration-dependence is discussed. Section 4 introduces the experimental setup used in this investigation. Section 5 presents EMA results of one flexible linkage of the planar parallel robot when the robot is stationary. Section 6 presents EMA results obtained for one flexible linkage of the planar parallel

robot, when robot linkage vibration is excited by rigid body motion. The configuration-dependency of structural vibration is discussed. Vibration control results are given in the paper. Finally, Section 7 concludes the paper.

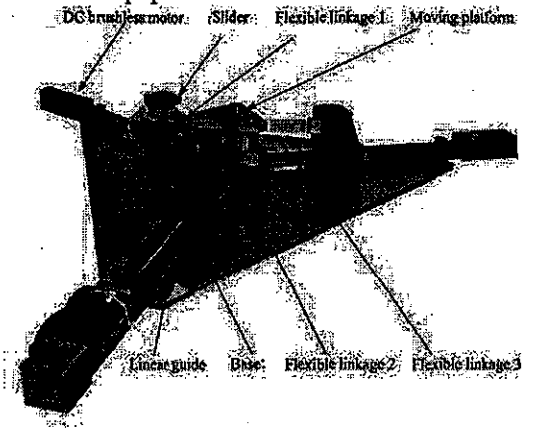

Figure 1.: A prototype of "Next Generation Parallel Robot"

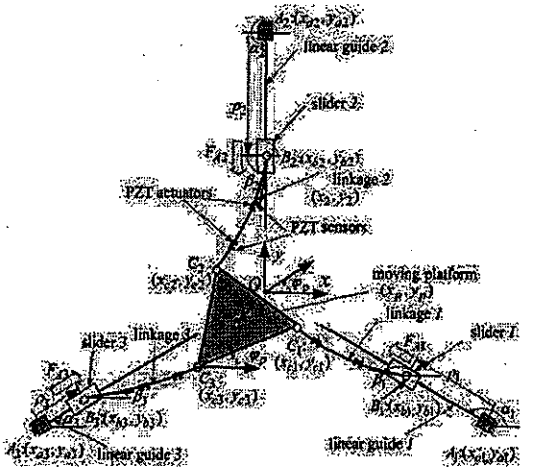

Figure 2.: Coordinate system for the "smart" planar parallel robot

2. EXPERIMENTAL MODAL ANALYSIS PROCEDURE

Here we review the Global Rational Fraction Polynomial (GRFP) Method, a frequency domain EMA procedure. The second subsection of the paper discusses the EMA theory of flexible mechanisms and the EMA methods using smart material sensors and actuators.

A. Global Rational Fraction Polynomial Method [16]

Experimental Modal Analysis (EMA) [17], a special case of system identification where an *a priori* model consisting of modal parameters is adopted, has been widely used in the experimental identification of structural dynamic characteristics. Generally speaking, the EMA methods can be classified into frequency-domain methods and time-domain methods [17]. Frequency domain methods extract mode properties from Frequency Response Functions (FRFs). Time domain methods extract mode properties from time-domain responses, i.e. Impulse Frequency Response Functions (IRFs). This subsection describes the GRFP modal analysis procedure, a widely used frequency domain modal analysis methods used in conjunction with the Eigensystem Realization Algorithm (ERA) [18], the Polyreference Frequency domain method [19], and the Complex Mode Indication Function (CMIF) method [20].

Providing a simple analysis technique, FRFs obtained using a traditional hammer and accelerometer as the actuator and sensor, defined here as a Type I FRF, are presented in this section. The essential element of frequency-domain modal identification is to use numerical techniques to identify the contribution of each vibration mode to one FRF. Obtained from this modal testing is a series of FRFs, usually represented by a column or a row vector of FRFs, with values at discrete frequencies. In order to identify modal properties, a Type I FRF resulting from the excitation of the k^{th} DOF to an output from an accelerometer, used as the sensor at the j^{th} DOF, may be written in a partial fraction form [17], so that contribution of each mode is obtained, i.e.,

$$\alpha_{jk}^{(I)}(\omega)=\sum_{r=1}^{N}\frac{-\{\phi_r\}_j\{\phi_r\}_k}{m_r(\omega_r^2/\omega^2-1+2i\omega_r\xi_r/\omega)}+R_{I_{jk}} \qquad (1)$$

where:

$m_r \triangleq$ modal mass for the r^{th} mode, $\omega_r \triangleq$ natural frequency for the r^{th} mode, $\xi_r \triangleq$ damping ratio for the r^{th} mode,

$\phi_r(x) \triangleq$ mode shape for the r^{th} mode, $j \triangleq$ index of the j^{th} degree of freedom, i.e. the ouput degree of freedom, $k \triangleq$ index of the k^{th} output degree of freedom, $^{(I)} \triangleq$ represents Type I FRF, $R_{I_{jk}} \triangleq$ residual inertia.

The GRFP method is used to fit measured FRFs to a rational polynomial form as follows, hence FRFs are written as:

$$\alpha_{jk}^{(I)}(\omega) = \frac{(b_0 + b_1(i\omega) + b_2(i\omega)^2 \cdots + b_{2N-1}(i\omega)^n)}{(a_0 + a_1(i\omega) + a_2(i\omega)^2 \cdots + a_{2M-1}(i\omega)^m)} \tag{2}$$

For an individual FRF $\alpha_{jk}(\omega)$, coefficients of polynomials in (2) may be determined with a least-squares formulation. For the frequency range of interest $[\omega_0, \omega_f]$, the error function for each FRF is,

$$J_{jk}^{(I)} = \mathbf{E}_{jk}^{(I)*T} \mathbf{E}_{jk}^{(I)} \tag{3}$$

where:

$\mathbf{E}_{jk}^{(I)} = \left\{(e_{\omega_0})_{jk} \quad (e_{\omega_1})_{jk} \quad \cdots \quad (e_{\omega_f})_{jk}\right\}^T$, $(e_{\omega_i})_{jk} \triangleq (b_0 + b_1(i\omega_i) \cdots + b_{2N-1}(i\omega_i)^n) - \tilde{\alpha}_{jk}^{(I)}(\omega_i)(a_0 + a_1(i\omega_i) \cdots + a_{2N-1}(i\omega_i)^m)$

In the GRFP method, all available FRFs are fitted simultaneously. The error function is the sum of $J_{jk}^{(I)}$ for all FRFs available. Direct identification of coefficients of the polynomials, using a least-squares GRFP formulation with rational polynomials, involves inversion of a Vandermonde matrix [17], which is ill-conditioned. Use of either orthogonal Forsythe [21], Chebyshev, or Legendre polynomials [17] avoids ill-conditioned matrices, with Forsythe polynomials used here. The coefficients in the following are determined, and then used to calculate rational polynomial coefficients in (2), i.e.,

$$\alpha_{jk}^{(I)}(\omega) = \frac{c_0 f_0(i\omega) + c_1 f_1(i\omega) + \cdots + c_{2N-1} f_{2N-1}(i\omega))}{d_0 f_0(i\omega) + d_1 f_1(i\omega) + \cdots + d_{2M-1} f_{2M-1}(i\omega))} \tag{4}$$

where: $f_{(k)}(i\omega) \triangleq$ the k^{th} Forsythe polynomial. After the rational polynomial coefficients are obtained using (2), the FRFs are converted from a form given by (2) to partial fraction forms as given by (1). Finally, natural frequency, damping ratio, and mode shape is calculated from FRFs in partial fraction form. In order to visualize mode shapes, mode shapes are usually normalized.

B. Literature Review on Experimental Modal Analysis of Flexible Mechanisms

The EMA techniques have been widely applied to identify structural dynamics, where rigid body motion is usually not involved. Theoretical and numerical simulation studies demonstrate that vibration characteristics of flexible mechanisms typically exhibit configuration-dependency and non-linearity, due to the coupling between vibration and nonlinear rigid body motion [22]-[23]. In a comprehensive review of multi-body system modeling [24], Shabana pointed out that development of experimental modal analysis techniques for multi-body systems could be one of "*the most challenging and interesting problems*" in the analysis of multi-body systems. Experimental modal identification is also critical for active vibration control of flexible multi-body system.

Traditional hammer and accelerometer excitation methods are practically impossible for use to identify vibration characteristics while a robot is moving. The emergence of distributed smart material components, including vibration transducers and signal processors, makes it possible for smart material transducers to be embedded or integrated to the host structure. This allows structural responses with distributed smart components to be monitored. Significantly, real-time analysis of modal properties of flexible mechanisms is also feasible. Saunders *et al.* [25] derived an EMA formulation for a simply supported plate with PZT actuators and PVDF sensors. Wang *et al.* [26] discussed the feasibility of modal testing using PZT transducers using a cantilever beam. In these investigations, the structures tested do not undergo rigid body motion, hence modal characteristics are linear and time-invariant. For many flexible multi-body systems, especially for flexible mechanisms, vibration characteristics are nonlinear and configuration-dependent. Hardage and Weins [27] used a hammer and an accelerometer to measure natural frequencies and damping ratios of a parallel robot when the robot is in different configurations,

and while the robot is stationary. In this paper, distributed PZT transducers are utilized to identify modal properties of a single flexible linkage of the planar parallel robot. The mode shapes at different configurations are also studied. Rigid-body motion is also used as the excitation for flexible deformation. The configuration dependency of modal properties is investigated by performing EMA with the planar parallel robot in different configurations.

3. DEVELOPMENT OF FRF FORMULATIONS FOR PZT TRANSDUCERS AND RIGID BODY MOTION EXCITATION

In this paper, in addition to an impact hammer, PZT actuators and voltage input to motors are used to excite structural vibration. In addition to accelerometers, PZT sensors are used as sensors. In this section, formulations of FRFs using PZT transducers and rigid body motion input are derived. In subsection A, the advantages and disadvantages of different sensing and actuation methods are discussed. In subsection B, the formulations using PZT transducers are derived. In subsection C, the formulations using rigid body motion input are developed.

A. Requirements on Exciting and Sensing of Vibrations in Flexible Mechanisms

Vibration tests have requirements on a number of aspects on vibration excitation, including (1) the bandwidth of excitation, (2) the location of excitation and (3) force output capability. Structural vibrations can be excited by an impact hammer, PZT patch actuators, or DC actuating motors. Both impact hammer and PZT actuator excitation methods have wide bandwidth. The advantage of an impact hammer is that it can be applied at different locations while PZT actuators are at fixed locations once bonded to the linkage surface. The advantage of PZT actuators is that they can be used for on-line modal identification and real-time control.

Rigid body motion during the operation of the parallel robot readily excites structural vibrations of flexible links, hence this approach can be used as an excitation source. The control effort during trajectory control has very limited bandwidth, as seen later in the paper. However, the rigid body trajectories used for excitation of structural vibrations emulates the operation of the platform during task execution.

Accelerometer and PZT sensors can be used to sense and identify structural vibration response. The advantages of using accelerometers is that the sensor can be easily relocated to other locations, therefore, displacement mode shapes can be extracted. However, in order to identify mode shapes using accelerometers without repeating a test many times, multiple accelerometers are required, however, use of Multiple accelerometers will add significant additional mass to the structures, altering the vibration response. The advantages of PZT patch sensors include: (1) fast dynamic measurement, (2) PZT sensors can be used during rigid body motion. In order to identify mode shapes, a relatively large number of PZT sensors are required. Therefore, PZT sensors should be made smaller so that multiple sensors can be used.

As stated above, with different characteristics, different combinations of excitation and sensing methods may be used, which provides comparison and validation for a single combination of transducers. In order to facilitate the use of these combinations, six FRFs are defined in Table I. Formulations for Type I FRF have been used in Section II. In order use Type II-VI FRFs are given in the Section B and C.

Table 1. Combinations of transducers

FRF Type	Input	Output
I	Impact hammer	Accelerometers
II	impact hammer	PZT Patches
III	PZT patch actuators	Accelerometers
IV	PZT patch actuators	PZT patch sensors
V	Rigid-body motion	Accelerometers
VI	Rigid-body motion	PZT Patches

B. Formulation of Modal Analysis Using PZT Transducers

In this work, PZT patches are used as actuators and sensors for EMA and active vibration control. In this section, FRF formulations for modal analysis using PZT patches are given.

1) PZT Patch Sensor and PZT Patch Actuator. According to the direct piezoelectric effect, a PZT patch sensor generates electric charges when subject to a strain. Using an impedance converter, the charge signal is converted to a voltage signal [28]. Correspondingly, termed the inverse piezoelectric effect, a PZT patch generates strain if voltages are applied. If these strains are constrained, forces or moments will be produced. Surface bonded PZT actuators generate a pair of bending moments between the actuators and the host structure [23], which are proportional to the applied voltage.

PZT sensors and actuators may exhibit hysteresis as other smart materials do, when large control signals are applied. The phenomenon must be taken into account when such PZT actuators are utilized for high precision positioning applications, such as nano-positioning. In this paper, the PZT actuators are used for a vibration suppression application, which has substantially less positional accuracy required as is required in motion control applications. Additionally, the voltages applied to the PZT actuators is not very high, reducing the effect of hysteresis in the PZT actuator response. Further, experimental results reported in this paper are the results of a number of tests conducted, averaged to reduce the effect of hysteresis in the response of the actuators.

2) Type II FRF. Type II FRFs are used to model point force input devices, such as an impact hammer, and PZT patches as sensors. This approach is used to determine mode shapes measured by PZT sensors and determine the sensitivity of PZT sensors.

Applied to a beam, strain is the second spatial derivative of elastic displacement; hence the response of a PZT patch is proportional to the second spatial derivative of the elastic displacement at the sensor location, which is the sum of the contributions of all modes, i.e.,

$$v_s = c_s \left.\frac{\partial^2 w}{\partial x^2}\right|_{x_s} \tag{5}$$

where: $v_s \triangleq$ voltage response of a PZT sensor, $c_s \triangleq$ sensitivity constant for a PZT sensor, $w \triangleq$ deflection of the beam, $x \triangleq$ coordinate of beam, $x_s \triangleq x$ coordinate of the midpoint of the PZT sensor.

From equations (1) and (5), an FRF describing transfer properties from a point force device at node k to a PZT patch sensor whose midpoint is at node j, defined here as Type II FRF, is expressed as,

$$\alpha_{jk}^{(\mathrm{II})}(\omega) = R_{F_{jk}} + \sum_{r=1}^{N} \frac{c_s \{\phi_r^{''}\}_j \{\phi_r^{'}\}_k}{m_r(\omega_r^2 - \omega^2 + 2i\omega\omega_r\xi_r)} + R_{I_{jk}}(\omega^2), \text{with } \phi_r^{'} \triangleq \frac{\partial^2 \phi_r(x)}{\partial x^2}. \tag{6}$$

3) Type III and Type IV FRFs. Type III and Type IV FRFs are both used to model a PZT patch as the excitation device. PZT patch actuators are used in the parallel robot for active vibration control, hence the influence of PZT patch actuators must be quantified through EMA. In order to perform EMA using PZT patch actuators, FRF formulations using PZT patch actuators are given. For Type III FRF, accelerometers are used as sensors, are used to determine the influences of PZT actuators. Type IV FRF with PZT patch sensors and actuators are used in the real-time control.

When a voltage is applied, a PZT patch actuator generates a bending moment in opposite directions at its two ends, indicated with subscripts as k_1 and k_2. An FRF from the PZT patch actuator voltage to an accelerometer sensor output, here defined as Type III, has the form,

$$\alpha_{jk}^{(\mathrm{III})}(\omega) = R_{F_{jk}} + \sum_{r=1}^{N} \frac{c_a \{\phi_r\}_j \left(\{\phi_r^{'}\}_{k1} - \{\phi_r^{'}\}_{k2}\right)}{m_r(\omega_r^2 - \omega^2 + 2j\omega\omega_r\xi_r)} + R_{I_{jk}}(\omega^2) \tag{7}$$

where: $c_a \triangleq$ coupling constant for the PZT patch actuator.

An FRF from the PZT patch actuator voltage to a PZT patch point sensor voltage, defined as Type IV, has the form,

$$\alpha_{jk}^{(\mathrm{IV})}(\omega) = R_{F_{jk}} + \sum_{r=1}^{N} \frac{c_s \phi_{jr}^{''} c_a (\phi_{k_1 r}^{'} - \phi_{k_2 r}^{'})}{m_r(\omega_r^2 - \omega^2 + 2i\omega\omega_r\xi_r)} + R_{I_{jk}}(\omega^2) \tag{8}$$

C. Excitation using Rigidbody Motion:

Type V and VI FRFs, particularly for robotic applications, are measured when the vibration of the

structure is excited by actuator drive motors. Type V FRFs measure linkage vibration using accelerometers and Type VI FRFs measure this vibration using PZT sensors. Driving signals are sent to actuator motors, which drive the rigid body motion of the robot. Vibration of the structure is excited due to coupling of rigid-body motion and linkage flexible deformation [23]. The coupling of rigid-body motion and flexible deformation is dependent on robot configuration.

For example, consider an un-damped dynamic system with one DOF rigid body motion $x_r(t)$ and one DOF flexible motion $x_e(t)$. The system dynamics is characterized by dynamic coupling amongst the rigid body coordinates through the nonlinear, configuration dependent terms in the inertia matrix M_{re}, [2]. In [2], the moving frame approach is used to derive a dynamic equation for a flexible link of the parallel robot and the parallel robot. Using the dynamic models of the flexible link and the parallel robot, it can be demonstrated that the coupling between the nonlinear rigid-body motion degrees of freedom and the flexible deformation is configuration dependent. Assuming no direct excitation on flexible deformation, only rigid body motion is excited by $F(t)$:

$$\begin{bmatrix} M_{rr} & M_{re} \\ M_{er} & M_{ee} \end{bmatrix} \begin{bmatrix} \ddot{x}_r(t) \\ \ddot{x}_e(t) \end{bmatrix} + \begin{bmatrix} 0 & 0 \\ 0 & K \end{bmatrix} \begin{bmatrix} 0 \\ x_e(t) \end{bmatrix} = \begin{bmatrix} F(t) \\ 0 \end{bmatrix} \tag{9}$$

where: $x_r \triangleq$ rigidbody motion displacement, $x_r \triangleq$ flexible deformation displacement, $M_{rr} \triangleq$ inertia for rigidbody motion, $M_{ee} \triangleq$ inertia for elastic motion, $M_{re}(x_r) = M_{er}^T(x_r) \triangleq$ configuration-dependent coupling of rigidbody motion and elastic motion, $F(t) \triangleq$ rigid body motion force input.

Performing a Fourier transformation on (9), we have,

$$-\omega^2 \begin{bmatrix} M_{rr} & M_{re} \\ M_{er} & M_{ee} \end{bmatrix} \begin{bmatrix} X_r(j\omega) \\ X_e(j\omega) \end{bmatrix} + \begin{bmatrix} 0 & 0 \\ 0 & K \end{bmatrix} \begin{bmatrix} 0 \\ X_e(j\omega) \end{bmatrix} = \begin{bmatrix} F(j\omega) \\ 0 \end{bmatrix} \tag{10}$$

Eliminating $X_e(j\omega)$, the FRF from the motor input to flexible deformation,

$$\frac{X_e(j\omega)}{F(j\omega)} = \frac{M_{er}/M_{rr}}{(M_{ee} - M_{er}^2/M_{rr})\omega^2 - K} \tag{11}$$

It can be seen from (11), that the eigenvalue of such a system can be shifted by $\sqrt{\frac{K}{M_{ee} - M_{er}^2/M_{rr}}} - \sqrt{\frac{K}{M_{ee}}}$.

For a configuration dependent system, M_{er} is configuration dependent. Hence the natural frequency exhibits configuration dependency.

$$\frac{X_r(j\omega)}{F(j\omega)} = \frac{1 + M_{ee}M_{re}\omega^2 / \left[(M_{rr}M_{ee} - M_{er}^2)\omega^2 - KM_{rr}\right]}{-M_{rr}\omega^2} \tag{12}$$

The rigid body mode has zero natural frequency, hence equation (12) becomes $\frac{1}{-M_{rr}\omega^2}$.

Type V frequency response functions from motor driving signal to an accelerometer attached to the structure are described as,

$$\alpha_{jk}^{(V)}(\omega) = \frac{-\omega^2 X_e(j\omega)}{F(j\omega)} = \frac{-M_{er}/M_{rr}}{(M_{ee} - M_{er}^2/M_{rr}) - K/\omega^2} \tag{13}$$

For a multi degree of freedom system with viscous damping, Type V FRF can be written as:

$$\alpha_j^{(V)}(\omega) = R_{F_{jk}} + \sum_{j=1}^{r} \frac{-c_j \{\phi_r\}_j}{m_r(\omega_r^2 - \omega^2 + 2i\omega_r\xi_r)/\omega^2} + R_{I_{jk}} \tag{14}$$

where: ω_r depends on robot configuration, c_j is the constant represnting sensitivity of an accelerometer. Similarly, Type VI FRFs from motor driving signal to a PZT patch sensor bonded to the structure are described as,

$$\alpha_j^{(VI)}(\omega) = R_{F_{jk}} + \sum_{j=1}^{r} \frac{c_s \{\phi_r\}_j}{m_r(\omega_r^2 - \omega^2 + 2i\omega\omega_r\xi_r)} + R_{I_{jk}} \tag{15}$$

D. Unified FRF Formulations

FRF formulations of Type I-VI, obtained in (1) and (6) to (15), have the following form,

$$\alpha_{jk}^{(m)}(\omega) = R_{F_{jk}} + \sum_{r=1}^{N} \frac{(R_{jk})_r}{(\omega_r^2 - \omega^2 + 2i\omega\omega_r\xi_r)} + R_{I_{jk}},\ m = I, II, III, IV, V, VI \tag{16}$$

where: $(R_{jk})_r \triangleq$ the residue of the r^{th} mode for $\alpha_{jk}^{(m)}(\omega)$.

These six types of FRFs are applicable to modal analysis procedures in Section 2.A. Using this procedure, $(R_{jk})_r$ are obtained, and from this, mode shapes are calculated. The mode shapes are in terms of displacement if accelerometers are used, or in terms of strain, if PZT patch sensors are used.

4. Parallel Robot Experimental Setup

The experimental planar parallel robot is introduced in this section. The experimental system is comprised of the planar parallel robot, a three-axis motion control system, active vibration control instruments, and a host PC with a MCX-DSP controller, which features 120 *MFlop/sec* to simultaneously perform motion and vibration control tasks. Using this setup, the results of experimental modal analysis and active vibration control experiments are given in Section 5 and Section 6.

Figure 2 shows a schematic of the smart planar parallel robot, whose architecture is categorized as a *P-R-R* (Prismatic-Revolute-Revolute) type, i.e. each of three kinematic chains is respectively comprised of a prismatic joint and two revolute joints in sequence. The three prismatic joints, i.e. the three sliders shown in Figure 2, are active joints, located at $B_i, i = 1,2,3$. Each slider is connected to a linkage through a passive revolute joint at $B_i, i = 1,2,3$. Three linkages are connected to the moving platform with a passive revolute joint at $C_i, i = 1,2,3$. Linkage *1* is made flexible while the other two are rigid. Both revolute joints at B_i and C_i are passive joints. Through actuation of the three DC motors, the moving platform, with a side length of $100mm$ and a mass of $4.049kg$, is driven to a desired location in the plane within the workspace, measuring approximately $40cm \times 40cm$. The parallel robot is designed to achieve a linear speed of 4 *m/s*, an acceleration of over $10g$, and a positioning accuracy of less than $10\,\mu m$.

In Figure 2, a global coordinate system is shown as (x, y, φ), with the origin of the coordinate system located at the center of the workspace, O. The position and orientation of the platform, at the mass center P, is defined as (x_p, y_p) and φ_p respectively. Three active prismatic joints, i.e. sliders, moves along ball screws, whose orientations are at angles α_i, measured with respect to the global x axis, respectively, 270°, 30°, 150°. The origins of three ball screws are indicated by $A_i, i = 1,2,3$. The coordinate from A_i to the location of the sliders B_i is defined as ρ_i, and used to denote the robot configuration in this paper. $\rho_i = 0,\ i = 1,2,3$ is the home configuration for the parallel robot. Each prismatic joint is driven by an *AeroTech* BM200 DC brushless motor. Assembled with this motor using a ball screw linear guide system, each slider comprises a prismatic joint. Motion control driving signals are generated by the *MCX-DSP* controller and conditioned as current signals by BAS320 amplifiers so that motors operate in torque (current) mode.

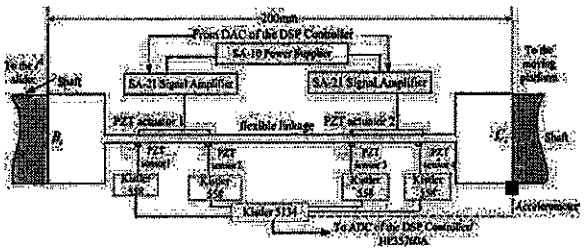

Figure 3.: Configuration of active vibration control system for one flexible link

Figure 4.: Locations to place the accelerometer

Figure 3 shows a schematic of the active vibration control system for the flexible linkage, denoted as linkage *1* in Figure 2. Four PZT sensors and two PZT actuators for active vibration control are bonded to this flexible linkage. A miniature *PCB A352C67* accelerometer is used to measure accelerations at different locations on the linkage. The charge signals from PZT sensors are converted to voltage signals by in-line Kistler 558 impedance converters. The voltage signal is then amplified to a desired level by a Kistler coupler 5134, which has a built-in low pass filter. These amplified signals are then sampled by the DSP unit. The DSP unit also provides PZT drive signals which are filtered by second order Butterworth low pass filters, with programmable bandwidth, and then amplified by an SA-21 signal amplifier, powered by an SA-10 power supply. An HP35670A dynamic signal analyzer, programmable by the host PC, is used to perform signal analysis and data logging.

5. Experimental Identification when the Robot is in a Stationary State

This section describes the experimental identification of the vibration modes of the flexible linkage in the planar parallel robot, when the robot is stationary. In Section 6, identification when the robot is excited by rigid body motion will be discussed. When stationary, no overall rigid body motion is involved and the structural dynamics of the robot may be treated as both linear and time-invariant for each configuration. PZT transducers and accelerometers are used in these tests. The placement of PZT sensors and actuators on the single flexible linkage is shown in Figure 3. During tests in which linkage vibration accelerations are measured, a miniature accelerometer is sequential placed at different locations over the beam, from point *1* to point *19* shown in Figure 4.

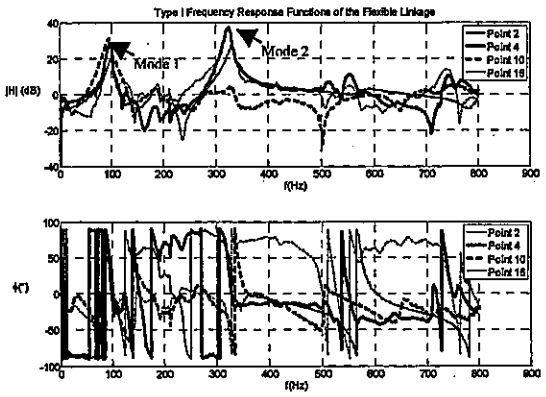

Figure 5.: Type I frequency response functions at locations 2. 4. 10. and 16

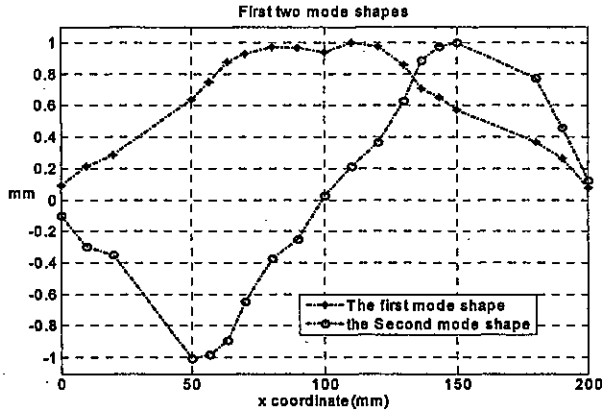

Figure 6.: First two mode shapes of the flexible linkage identified using Type I FRFs

Extensive modal identification experiments have been performed on linkage *1* shown when the linkage is stationary, i.e., when servo motors are locked so that there is no overall rigid body motion involved. Type I, II, III, and IV FRFs are used to identify linkage mode shapes. Type IV FRFs are acquired and analyzed at two different configurations to investigate the configuration dependency of linkage mode shapes. Analysis of Type I, II, FRFs is introduced in Section A. Analysis of Type III FRFs is introduced in Section B. Type IV FRFs and their configuration-dependency are introduced in Section C.

A. Identification Using Type I and Type II FRFs

Type I FRFs defined in Section 2 are used to identify the linkage mode shapes at the home configuration, i.e. three motors are locked with the platform located at the center of the workspace. During these tests, an accelerometer is placed sequentially from point *1* to point *19* (shown in Figure 4) and the impact hammer is used to excite the linkage at point *18*. These points are chosen so they are evenly distributed along the length of the link. For each accelerometer location, the test is performed ten times, taking the average result. For the purpose of illustrating our results clearly, Figure 5 shows Type I FRFs determined at five locations, i.e. points *2, 4, 10, 16,* which describe transfer properties from the

point of excitation (location 18) to these points. Other FRFs have similar characteristics to these five plots. Using these FRFs, the first two mode shapes are identified using the GRFP procedure described in Section 2, and are shown in Figure 6. The first natural frequency is 94.14Hz with a damping ratio of 2.4 %. The second natural frequency is 323.71Hz with a damping ratio of 1.07% .

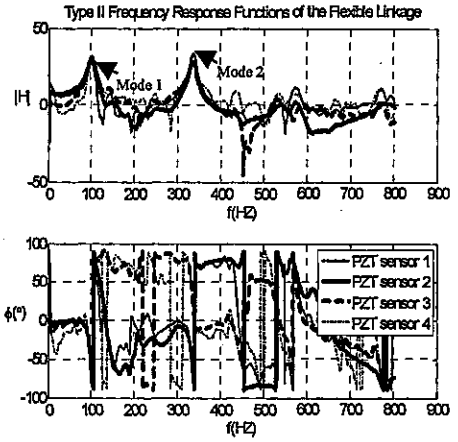

Figure 7.: Type II FRFs of the flexible linkage at the home configuration

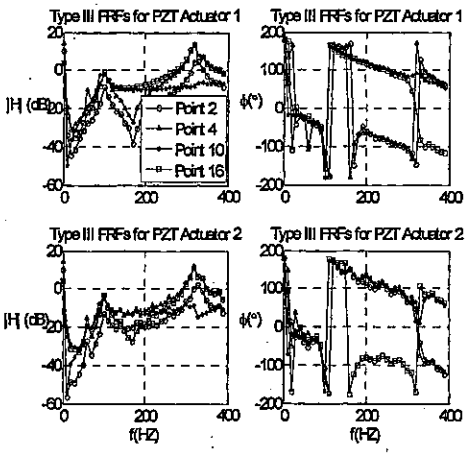

Figure 8. Type III FRFs of the flexible linkage at the home configuration

Type II FRFs, shown in Figure 7, are also used to identify the linkage mode shapes at the home configuration. PZT sensors on the linkage are used to record the outputs when an impact hammer excites the linkage at point *18*. The natural frequencies and damping ratios obtained are close to those obtained from Type I FRFs. Mode shapes are found to be similar to the second derivatives of mode shapes from Type I. This is consistent with the theory that acceleration FRFs give displacement mode shapes and PZT sensors give strain mode shapes.

B. Identification Using Type III FRFs

Using PZT actuators *1* and *2,* shown in Figure 4, to excite the beam, and an accelerometer sequentially placed on point *1* to point *19* to measure vibration signals, Type III FRFs, from PZT actuators to nineteen points, are acquired. Again, to permit the results to be seen readily, five FRFs from PZT actuator *1* to point *2, 4, 10,* and *16* are shown in Figure 8.

Following the GRFP procedure in Section 2, analysis of these FRFs gives mode shapes shown in Figure 9, which are consistent with the results of Figure 5. Through identification using Type III FRFs, the modal coupling factors [17] of PZT actuators with the host linkage are determined, which will be used in active vibration control design to follow.

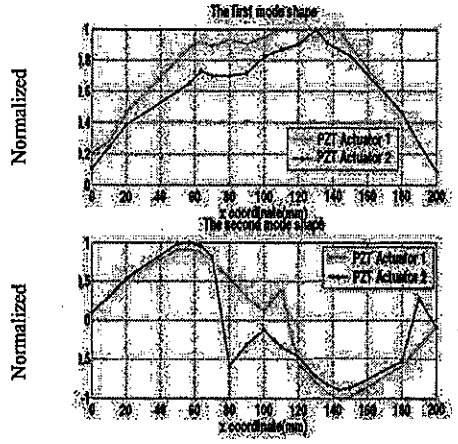

Figure 9.: Mode shapes identified from Type III FRFs in Figure 8

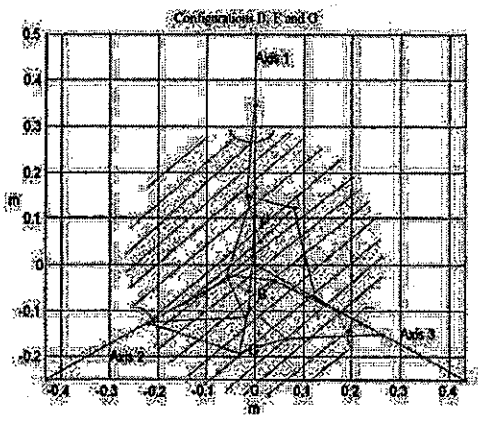

Figure 10.: Configurations *B*, *F*, and *G* of the parallel robot

C. Identification Using Type IV FRFs

Type IV FRFs, using the combination of a PZT actuator and PZT sensors, are acquired in different robot configurations, to investigate the linkage mode shapes and their configuration dependency. Configuration B and configuration F are the configurations used to demonstrate these results. In the joint space, the coordinates for B and F are respectively $\{-52.31,\ 33.45,\ 32.56\}mm$ and $\{80.25,\ -34.20,\ -40.69\}mm$ as shown in Figure 10, in which the relative position of the platform in the workspace is plotted. At configurations B and F, the center of the moving platform is 17.4cm apart.

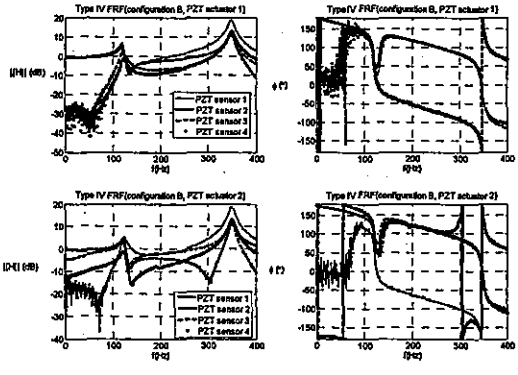

Figure 11. : Type IV FRFs measured at configuration B and F

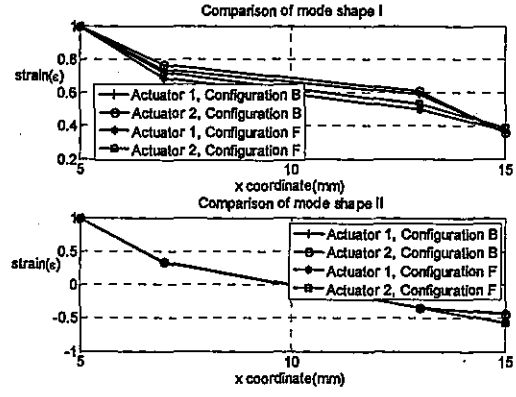

Figure 12.: Mode shapes identified from Type IV FRFs at configurations B and F

Figure 11 shows Type IV FRFs when PZT actuator *1* and *2* are used to excite the flexible linkage when the parallel robot is at configuration B and F. The analysis of Type IV FRFs give the mode shapes at these two configurations, as shown in Figure 12, and the mode coupling factors of PZT actuators. The mode shapes, derived from the output of PZT sensors, are in the terms of strain. Through analysis, it is found that strain mode shapes are approximately proportional to the second derivative of the displacement mode shapes in Figure 9. From Figure 12, it is observed that the linkage mode shapes, determined when the robot is stationary, are very similar for the different configurations tested, especially for mode *2*. There are also differences amongst the natural frequencies identified. For example, while the first natural frequency identified using PZT actuator *1* at configuration B is 119.4Hz, the first natural frequency identified using PZT actuator *2* at configuration F is 125.0Hz. This shows that the modal frequencies of the linkage are configuration-dependent. Here the configuration dependency is attributed to the variation in the constraints at the linkage boundaries.

6. Identification of Flexible Motion Caused by Rigid-body Motion Input

In Section 5, EMA tests are performed with several combinations of transducers while the robot is stationary. In this Section, identification of flexible deformation while the robot undergoes rigid-body motion is introduced. During rigid body motion, vibration modes are coupled with rigid body motion and nonlinear terms in the dynamic equation affects the system motion [2]. This also has been demonstrated using Equation (11) in Section 3. In order to model the influence of rigid body motion on linkage flexible motion, frequency response functions from the motor voltage to linkage vibration caused are measured and analyzed. FRFs between motor voltage and linkage vibration can be measured in two ways:

The first method is to measure FRFs when the robot vibration is excited by a short-distance high-acceleration rigid body motion input. Note that the linkage dynamics, i.e. FRFs change during the motion. However, FRFs can be assumed to be constant if the rigid body motion is very small. The advantage of the method is that the measured data reflect a real situation, i.e. pick-and-place task execution. The disadvantage of the method is the excitation is confined to a low frequency range, as shown in Figure 13.

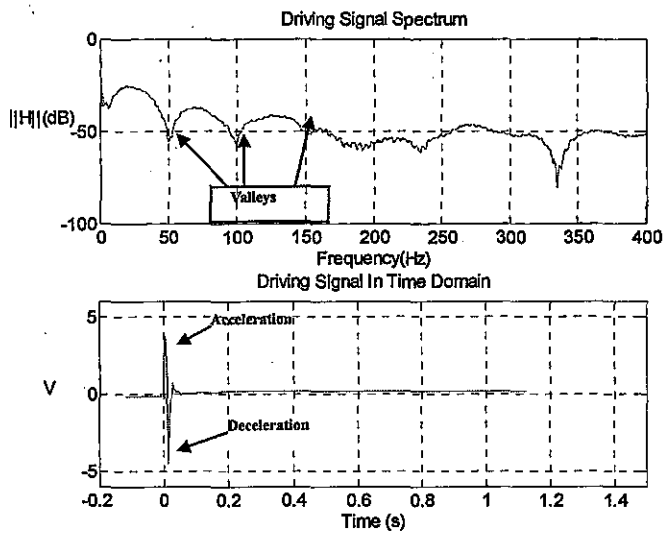

Figure 13.: Excitation from motor driving signal

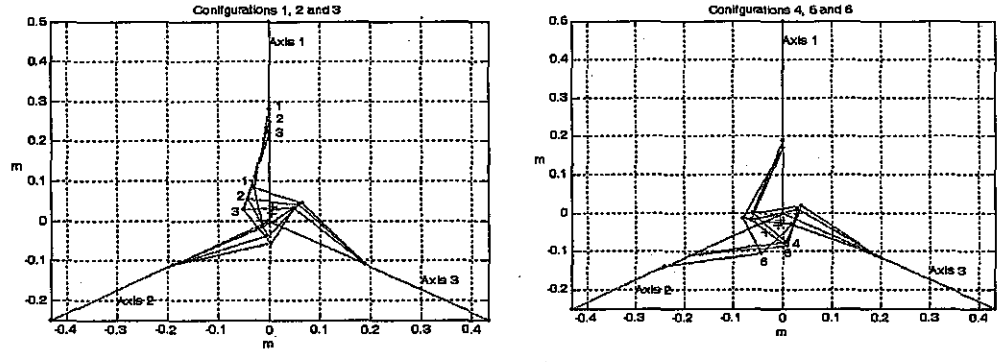

Figure 14: Configurations 1-6

The second method is to input low-level random signals (i.e.1V-2V) to the drive motors, hence the rigid body motion has very small amplitude, and the FRFs are assumed to be constant. Using this method, the bandwidth of the input can be set through a random signal generator. Section A introduces the identification during rigid body motion control. Section B describes the identification process when random signals are used. Based on these identification results, transfer function for motor voltage input is simplified. Finally, vibration control results are given in Section D.

More than twenty different robot configurations have been tested. These configurations are widely distributed in the workspace. Some of these tests are performed using several different combinations of transducers, which give consistent results. The experimental results have been shown to exhibit a high degree of repeatability. The results presented in this paper are representative of the tests performed, however most of these results are not included in the paper due to limited paper length.

A. Identification of Modal Properties During Rigid Body Motion

In this subsection, motors inputs during short-distance high-acceleration rigid body motion are used as the excitation source of linkage vibration. The FRFs from motor inputs to PZT sensor responses are fitted to estimate modal properties of the flexible linkage when the robot is moving. Shown in Figure 14, six configurations are numbered from 1 – 6, denoted by $\mathbf{q} = \{\rho_1 \quad \rho_2 \quad \rho_3\}$ where ρ_i have units of mm, are respectively selected as: $\mathbf{q}^1 = \{0 \quad 0 \quad 0\}$, $\mathbf{q}^2 = \{30 \quad 0 \quad 0\}$, $\mathbf{q}^3 = \{60 \quad 0 \quad 0\}$, $\mathbf{q}^4 = \{-30 \quad 0 \quad 0\}$, $\mathbf{q}^5 = \{-50 \quad 0 \quad 0\}$, and $\mathbf{q}^6 = \{-50 \quad 60 \quad 10\}$.

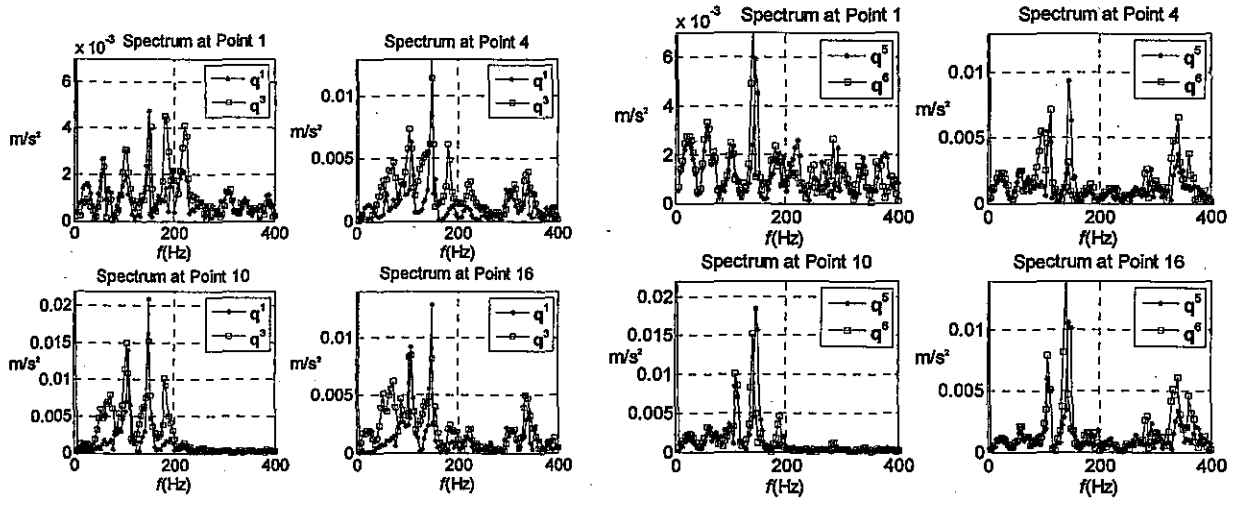

Figure 15.: Linkage acceleration spectrum during 5-mm translation of axis 1

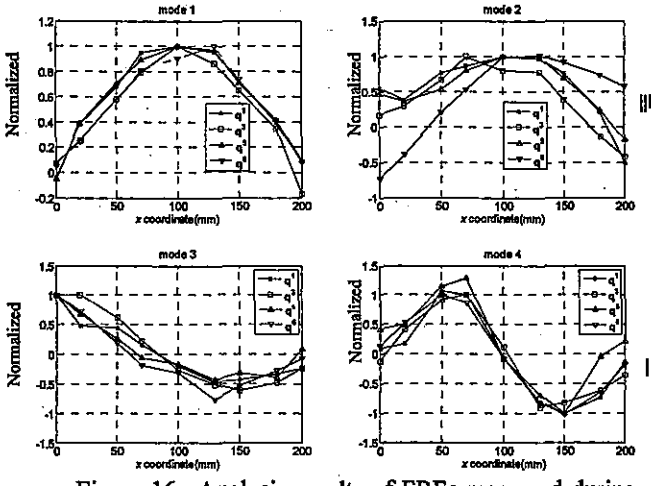

Figure 16.: Analysis results of FRFs measured during rigid body motion control

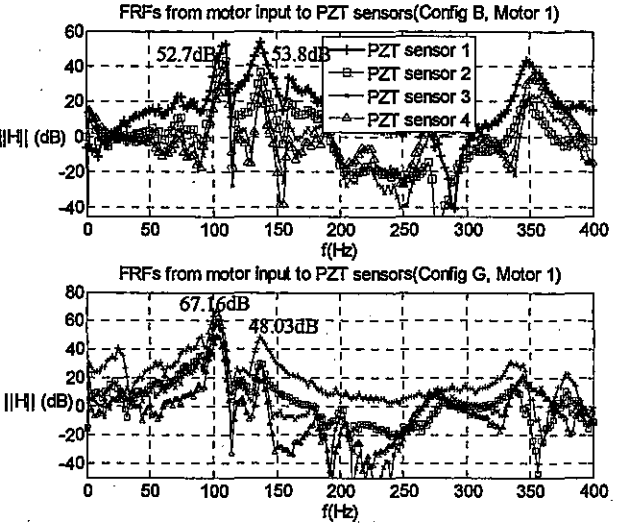

Figure 17: FRFs at Configurations *B* and *G*

Measurements at configuration 1, 3, 5, and 6 are plotted Figure 15. When the robot is positioned at these configurations, a position input command of 5 mm is given to axis 1. Figure 15 shows acceleration spectrums at nine locations. It can be observed from Figure 15 that: (1) the configuration dependency of FRFs is very substantial; (2) the measured signals are not smooth due to the excitation energy being within a low frequency range. The FRFs from the above cases are used to perform EMA. From the figure, we can observe the amplitudes of FRFs are strongly dependent on robot configuration. Peak frequencies are also dependent on configuration, however, less significantly than amplitudes. Among many peaks in Figure 15, there are some peaks caused by valleys in the frequency spectrum of the driving signal, which will be eliminated based on subsequent analysis. To eliminate these pseudo modes requires a significant effort. During EMA, four most significant modes are identified.

Figure 16 shows these four normalized modes. In the experimental modal analysis, some peaks of FRFs close to each other exhibit very similar mode shapes. Here only physically meaningful mode shapes are plotted. The first and the forth modes are basically the first two modes for a pinned-pinned beam, i.e. the mode shape vector in the stationary state is a subset of that during rigid body motion. The

second mode resembles the first mode for a pinned-free beam, which is very likely caused by the mobility of the moving platform. The third mode resembles the first mode for a free-pinned mode, which is assumed to result from the lateral flexibility of ball screws, which convert motor rotation to translation of sliders. Pinned-pinned mode shapes are exhibited in other configurations when the robot is stationary. Since the results shown in Fig. 16 are obtained in four different configurations using high acceleration, short-displacement motion to excite structural vibrations, it can be concluded that these same mode shapes exhibited in the stationary states are also exhibited when structural vibration is excited by high acceleration short-displacement rigid-body motion. In summary, analyses of FRFs excited by short-displacement rigid body motion at different configurations give two modes not seen in stationary states in addition to two modes appearing during stationary tests.

The similarity of the two pinned-pinned modes is discussed in the following, making use of the dynamic model developed using the moving frame approach in [2]. In the moving frame approach, the flexible deformation is defined in the body-fixed frame; hence the linear mode shape is used. The configuration-dependency is the result of the coupling of nonlinear rigid body motion and flexible deformation. The other two vibration modes result from other flexible mechanical components of the parallel robot, such as the ball-screws. We note that the natural frequencies of these two pinned-pinned modes might be affected by geometric stiffening caused by the axial loads on the flexible linkages during motion of the platform. In this paper, the stiffening phenomenon is not considered because it has a very limited effect on the frequencies, i.e. within 1-2%.

B. Identification of Linkage Modal Properties Using Random Input to Motors

In order to overcome the difficulties accompanying the limited bandwidth of the actuator motor used for excitation of structural vibration, discussed in Section 5, random motors inputs are used as the excitation source of linkage vibration. The FRFs from motor inputs to PZT sensor responses are fitted to estimate modal properties of the flexible linkage when the robot is excited with random input signals applied to the drive motors. Band-limited white noise signals have constant energy distribution over the selected frequency range so that valleys in Figure 13 can be avoided. A random signal is input to three motors of the parallel robot when the robot is at different configurations so these results could be better compared.

Figure 17 shows FRFs from motor 1 to PZT sensors 1,2,3, and 4 at configuration B (joint space coordinate $(-52.3,\ 33.5,\ 32.6)mm$) and configuration G (joint space coordinate $(-115.3,\ 34.5,\ 83.8)mm$). These three configurations are plotted in Figure 10. The natural frequencies identified at configurations B , F and G are given in Table 2. Strain mode shapes identified at configuration B and configuration G are shown in Figure 18.

Table 2: Natural frequencies identified at configuration B, F and G

	Natural frequency for mode 1	Natural frequency for mode 2	Natural frequency for mode 3
Configuration B	107.88Hz	136.27 Hz	350.23Hz
Configuration F	105.92Hz	132.71Hz	341.84Hz
Configuration G	103.39Hz	136.31Hz	340.82Hz

From these FRF plots, we can see the shapes of the FRFs are quite different from each other, with the amplitudes of peaks varying significantly and the natural frequencies varying relatively less significantly. The contribution of the third mode, at approximately 200Hz, is much less significant than the second mode, as well as the other two modes. The natural frequencies at two configurations are different from each other, as shown in Table 1, especially the second mode. However, the mode shape vectors at these two configurations are very similar. The similarity of mode shape vectors is demonstrated by Figure 16 and 18, which allows assumptions that can be used to simplify the active vibration control design. The simplification process will be discussed in the following Sections C.

C. Simplification of Transfer Function

From observations in Section A and B, four modes in Figure 16 can be classified into two groups: (1) two pinned-pinned modes, i.e. mode 1 and mode 4 (2) pinned –free and free-pinned modes, i.e. mode 2 and mode 3. For the two pinned-pinned modes, the change of mode shapes and natural frequencies at different configurations is insignificant and may be demonstrated by evaluating equation (11). The lack of sensitivity of mode shapes to configuration means the vibration patterns remain quite similar. However, the configuration-dependency is very significantly exhibited in the amplitudes of the FRFs. This configuration-dependency can be demonstrated using a dynamic model developed using the moving frame approach [2]. Flexible body dynamics can be modeled using linear vibration theory, hence the mode shapes are constant. However, the coupling of flexible body deformation with rigid body motion is nonlinear, hence highly dependent on robot configuration, which results in the configuration dependent modal controllability or accessibility [29]. Solving the eigenvalue problem using the configuration-dependent inertia matrix and constant stiffness matrix, results in an eigen-frequency, which is configuration dependent.

It is observed that linkage mode shapes for the two pinned-pinned modes are nearly identical although they are extracted from the configuration-dependent FRFs from motor voltage input to linkage vibration response. In order to evaluate the possibility of control of configuration-dependent vibration with linear-time invariant mode shapes, an assumption is made here to separate the transfer functions from motor voltage input to PZT sensor responses $\mathbf{G}(s)$ into contributions from mode 2. $\mathbf{T}(s)$ and contributions from the first pinned and the second pinned-pinned modes, which can be further regarded as the product of configuration-dependent coefficient $\mathbf{O}(\mathbf{q})$ and linear constant linkage dynamics $\mathbf{H}(s)$:

$$\mathbf{G}^T(s) = \mathbf{T}(s) + \mathbf{O}(\mathbf{q})\{H_1(s) \quad H_2(s) \quad H_3(s) \quad H_4(s)\} \tag{17}$$

where: $H_i(s) = \sum_{j=1,4} \frac{c_j \varphi_i^{(j)}}{s^2 + 2\xi_j \omega_j s + \omega_j^2}$, $i = 1,2,3,4$, $T_i(s) = \sum_{j=2,3} \frac{c_j \varphi_i^{(j)}(\mathbf{q})}{s^2 + 2\xi_j \omega_j(\mathbf{q}) s + \omega_j^2(\mathbf{q})}$, $i = 1,2,3,4$

$c_j \triangleq$ motor-voltage infleunce factor for the j^{th} mode, $\varphi^{(j)} \triangleq$ the j^{th} mode shape.

Note that the configuration-independent contribution of the two pinned-pinned modes is included in $\mathbf{H}(s)$. The configuration-dependent contribution of two pinned-pinned modes is included in $\mathbf{O}(\mathbf{q})$. The contribution of the remaining modes, such as the second mode, is included in $\mathbf{T}(s)$. Note that the simplified transfer function, is related to the second partial derivative of the jth mode shape, which may be explained using Equation (8).

D. Active Vibration Control Design

The assumption made in Section C allows the separation of $\mathbf{G}(s)$ into $\mathbf{T}(s)$, $\mathbf{O}(\mathbf{q})$ and $\mathbf{H}(\mathbf{s})$. A modal domain vibration control algorithm to modify the poles of $\mathbf{H}(\mathbf{s})$ is designed. A linear mode controller has three parts [30]: (1) the modal observer [4], which extracts modal coordinates from time domain responses of PZT sensors; and is based on modal vectors previously identified (2) the modal controller, which calculates control effort in the modal domain based on modal coordinates; (3) the modal synthesizer, which calculates the time-domain control effort based on the control effort in the frequency-domain. Further description of modal domain control can be found in [4]. The advantage of a modal controller is the resultant decoupling of modes, permitting the modal controller to be designed targeting individual modes.

In the design of the controller for mode 1 $\{0.74 \quad 0.48 \quad 0.38 \quad 0.28\}$ and mode 2 $\{0.86 \quad 0.3 \quad -0.21 \quad -0.36\}$, the first-and second order pinned-pinned strain modal vectors identified at configuration B as shown in Figure 18, are used to construct a modal filter [4]. In order to increase modal damping, a derivative modal control law is used [30]. In Figure 19, FRFs from the motor input to four PZT sensors, using derivative control gains for the first and the second pinned-pinned modes, are compared with the FRFs for the case in which vibration control is not used. It is observed that vibration amplitudes of these two modes are substantially reduced. Multi-mode control and gain-scheduling control for different manipulator configurations are currently under investigation.

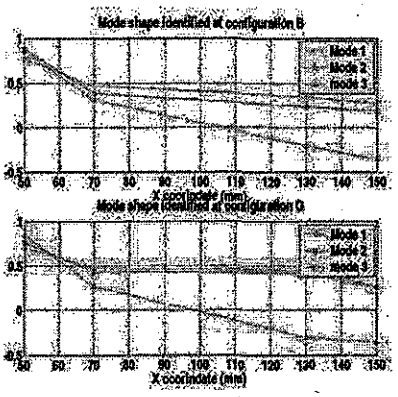

Figure 18.: Mode shapes identified from FRFs in Figure 17

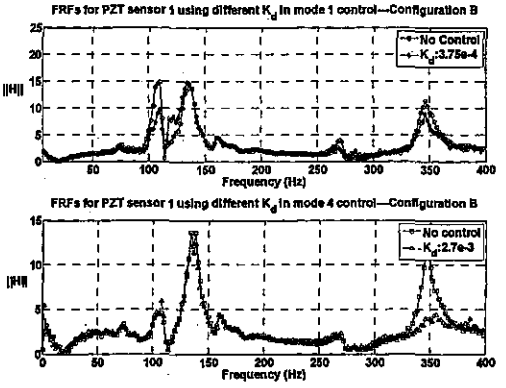

Figure 19.: Derivative modal control for two pinned-pinned modes

7. Conclusion

This work has focused on the investigation of the characteristics of this structural vibration utilizing distributed Lead Zirconate Titanate (PZT) transducers and rigid body motion. The main contribution of this paper is to identify configuration-dependent vibration characteristics of a flexible linkage in a parallel robot using smart material transducers and provide a foundation for the development of active vibration control. EMA of the flexible linkage dynamics are undertaken when the planar parallel robot is in both a stationary state and during rigid body motion. Displacement mode shapes of the flexible linkage using hammer-accelerometers tests, found to be consistent with those using PZT transducers, are determined to be weakly configuration dependent. In contrast, the influence of rigid body motion on linkage flexible motion, i.e. the vibration characteristic of parallel robot, is determined to be strongly configuration dependent. The mode shapes identified while the robot is stationary are found to be subsets of those identified during rigid body motion. Based on experimental observations, we make the assumption that the influence of rigid body motion on flexible linkage motion may be separated into a configuration dependent part and a configuration independent part. A linear mode controller is designed with the resultant control results presented.

8. REFERENCES

[1] L.W.Tsai, *Robot Analysis: The Mechanics of Serial and Parallel Manipulators*, John Wiley & Sons, New York, N.Y., 1999.

[2] X. Wang, J.K. Mills, "Dynamic modeling of a flexible-link planar parallel platform using a substructuring approach", *Journal of Mechanisms and Machine Theory*, Vol.41, No. 6, pp. 671-687, 2006.

[3] I. Heerah, B. Benhabib, B. Kang, J.K. Mills, "Architecture selection and singularity analysis of a three degree-of-freedom planar parallel manipulator", *the Journal of Intelligent and Robotic Systems: Theory and Applications*, Vol. 37, No. 4, , pp. 355-374, 2003.

[4] R.L. Clark, W.R. Saunders, G.P. Gibbs, *Adaptive Structure: Dynamics and Control*, John Wiley & Sons, 1998.

[5] W.L. Cleghorn, F.G. Fenton, B. Tabarrok, "Optimal design of high-speed flexible mechanisms", *Mechanism and Machine Theory*, Vol. 16, No. 4, pp.339-406, 1981.

[6] A. Ghazavi, F. Gardanine, "Dynamic analysis of a composite material flexible robot arm", *Computer and Structure*, Vol. 49, No. 2, pp. 315-325, 1981.

[7] E.H. El-Dammah, S.H.Farghaly, "Vibratory response of a sandwich link in a high-speed mechanism", *Mechanism and Machine Theory*, Vol. 28, No. 3, pp. 447-457, 1981.

[8] N.C. Singer, W.P. Seering, "Design and comparison of command shaping methods for controlling residual vibration", *Proceedings of IEEE International Conference on Robotics and Automation*, pp. 888-893, Cincinnati, Ohio, USA, 1989.

[9] C.K. Sung, Y.C. Chen, "Vibration control of the elastodynamics response of high-speed flexible linkage mechanisms", *ASME Journal of Vibration and Acoustics*, vol. 113, pp. 14–21, 1991.

[10] C.Y. Liao, C.K. Sung, "An elastodynamic analysis and control of flexible linkages using piezoceramic sensors and actuators", *ASME Journal of Mechanical Design*, vol. 115, pp. 658 –665, 1993.

[11] S.B. Choi, C.C. Cheong, B.S. Thompson, M.V. Gandhi, "Vibration control of flexible linkage mechanisms using piezoelectric films", *Mechanism and Machine Theory*, vol. 29, no.4, pp. 535-546, 1994.

[12] S. Yuan, Q. Xu, L. Zhang, "Experiments on active vibration control of a flexible four-bar linkage mechanism", *ASME Journal of Vibration and Acoustics*, vol. 122, pp. 82 –85, 2002.

[13] X. Zhang, C. Shao, A.G. Erdman, "Active vibration controller design and comparison study of flexible linkage mechanism systems", *Mechanism and Machine Theory*, vol.37, no.9, pp. 985-997, 2002.

[14] B.S. Kang, J.K. Mills, "Dynamic modeling of structurally-flexible planar parallel manipulator", *Robotica*, Vol. 20, No. 3, pp. 329-339, 2002.

[15] García de Jalón J, Bayo E, *Kinematic and Dynamic Simulation of Multibody Systems: The Real-Time Challenge*, Sringer-Verlag Press, 1994.

[16] M.H. Richardson, D.L. Formenti, "Global fitting: an efficient method of experimental modal analysis", *Proceeding of International Modal Analysis conference III*, vol.1, pp.390-397, 1985.

[17] D.J. Ewins, *Modal Testing: theory, practice and application*, Research Studies Press, 2000.

[18] M.T. Chuang, S.Y. Chen, Y.G. Tsuei, "Modal parameter identification by eigensystem realization algorithm", *Proceedings of the 15th International Modal Analysis Conference*, vol.1., pp. 41-49, Orlando, FL, USA, February 3-6 1997.

[19] M. Bensaibi, C. Gontier, "A comparison between a time domain and a frequency domain identification method", *Proceedings of the Tenth International Congress on Sound and Vibration*, vol.1., pp. 4417-4426, Stockholm, Sweden, July 7-10, 2003.

[20] W. Leurs, F. Deblauwe, F. Lembregts, "Modal parameter estimation based on complex mode indicator functions" *Proceedings of SPIE .- The International Society for Optical Engineering*, vol.1923, no. 2, pp. 1035-1041, February 1-4 , 1993.

[21] H. Van der Auweraer, J. Leuridan, "Multiple input orthogonal polynomial parameter estimation", *Mechanical Systems Signal Process.*, vol. 1, pp. 259—272, 1987.

[22] A. Midha, D. Karam, D., B.S. Thompson,, 'Elastic slider-crank mechanism. A study of the intrinsic configuration-dependent modal properties", in *Proceedings of 22nd Biennial* Mechanisms Conference, pp. 337-346, 1992.

[23] X. Wang, J.K. Mills, "FEM dynamic model for active vibration control of flexible linkages and its application to a planar parallel manipulator", *Journal of Applied Acoustics*, Vol.66, No.10, pp.1151-1161, 2005.

[24] A.A. Shabana, "Flexible multibody dynamics: review of past and recent developments", *Journal of Multibody System Dynamics*, vol.1, no. 2, pp.189-222, 1997.

[25] W.R. Saunders, D.G. Cole, H.H. Robertshaw, "Experiments in piezostructure modal analysis for mimo feedback control", *Smart Material and Structures*, no.3, , pp. 210-218, 1994.

[26] B.T. Wang, C.C. Wang, "Feasibility analysis of using piezoceramic transducers for cantilever beam modal tesing", *Smart Material and Structures*, no.6, pp. 106-116, 1997.

[27] D.S. Hardage, G.J. Wiens, "Modal analysis and modeling of a parallel kinematic machine", *IMECE Proceedings of the ASME: Manufacturing Science and Engineering*, Nashville, TN, MED-vol. 10, pp. 857-862, November 14-19, 1999.

[28] A. J. Fleming, S. O. R. Moheimani, "Improved current and charge amplifiers for driving piezoelectric loads, and issues in signal processing design for synthesis of shunt damping circuits", *Journal of Intelligent Material Systems and Structures*, vol. 15, no. 2, pp. 77-92, 2004.

[29] J. Cheong, Y. Youm, W.K. Chung, "Investigation and comparison of possibleboundary conditions and system vibration modes in two-link flexible manipulators", *Proceedings of ASME International Mechanical Engineering Congress and Exposition*, Vol. 2,pp. 1805-1812 New York, NY, United States, 2001.

[30] L. Meirovitch, "On the implementation of modal filters for control of structures", *Collection of Technical Papers - AIAA Guidance and Control Conference.*, Seattle, WA, USA, pp. 624-636, 1984.

[31] G. Song, S.P. Schmidt, B.N. Agrawal, "Experimental study of active vibration suppression of flexible structure using modular control patch", *Proceeding of IEEE Aerospace Applications Conference*, Vol. 1, pp. 189-201, Los Alamitos, CA, USA, 1998.